The effect of solution chemistries and freezing temperatures on the morphology of cryogenic opal-A (COA): implications for past climates on Mars

J.V. Hogancamp[a], T.J. Lapen[b], H.S. Chafetz[b], Elsenousy, A.[c]

[a] Geocontrols Systems – JETS Contract at NASA Johnson Space Center, Houston TX, 77058.

[b] Houston Department of Earth and Atmospheric Sciences, University of Houston, Houston, TX 77204-5007.

[c] Department of Earth Sciences, University of California Riverside, Riverside, CA 92521.

Corresponding author: Joanna Hogancamp (joanna.hogancamp@nasa.gov)

Highlights:

- Cryogenic opal-A made in H_2SO_4 solutions is more angular than COA made in HCl solutions.
- Cryogenic opal-A particle size decreases with decreasing freezing temperature.
- Cryogenic opal-A morphology may provide clues about past climate and geochemistry on Earth and Mars.

Abstract

Cryogenic opal-A (COA) is a type of hydrated amorphous silica that forms when silica-rich geothermal fluids erupt sub-aerially and are exposed to air temperatures below 0 °C. As the fluid cools and water-ice forms, the solution increases in ionic strength and reaches saturation of opal-A. This results in the precipitation of opal-A between water ice crystals. Natural COA is found embedded within frozen fluids near hydrothermal sources, and has been shown to preserve signs of biological activity. In this study, two solution chemistries (hydrochloric acid (HCl) and sulfuric acid (H_2SO_4)) and three freezing temperatures (-20, -80, -196 ºC) were used to synthesize COA in the lab. SEM analyses showed that COA frozen at -20 ºC in HCl solutions produced smooth silica branches similar to what was observed in previous studies. COA precipitated at lower freezing temperatures demonstrated progressively smaller particle sizes and unique morphologies such as halite dendrites within silica, desiccation cracks, and pores. COA made in H_2SO_4 solutions was more angular and fragmented than COA made in HCl solutions. Particle size also decreased with decreasing freezing temperature. COA textures have implications for terrestrial samples as well as future samples returned from Mars because they can provide information about past climate and fluid chemistry.

Plain Language Summary

Cryogenic opal-A (COA) is a hydrous silicate material that can form when geysers and hot springs erupt and are exposed to air temperatures below 0 °C. COA forms in brine veins that are between water ice crystals and takes the shape of the veins in which they form. COA has been shown to preserve signs of biological activity. In this study, two solution chemistries (hydrochloric acid (HCl) and sulfuric acid (H_2SO_4)) and three freezing temperatures (-20, -80, -196 ºC) were used to form COA in the lab. Scanning electron microscope analyses showed that, in general, COA particle size decreased with decreasing freezing temperature. Additionally, COA made in HCl solutions were smooth and tubular whereas COA made in H_2SO_4 solution were angular and fragmented. COA textures have implications for terrestrial samples as well as future samples returned from Mars because they can provide information about past climate and fluid chemistry.

Keywords: Opal-A; cryogenic; hydrothermal; Mars; silica.

1 Introduction

Opal-A is a noncrystalline form of opal (SiO_2*nH_2O) that consists of silica with water that is adsorbed, trapped in voids, or occurring as silanol groups (Si-OH). On Mars, opal-A has multiple proposed formation mechanisms including low-temperature hydrolysis of basalt, precipitation from hot springs or geysers, and acid-sulfate leaching of basalts from fumarole steam condensates (McAdam et al., 2008; Squyres et al., 2004; Ruff et al., 2011). In Mars-analog hydrothermal systems such as in the Yellowstone National Park, Wyoming, or at Rio Tinto, Chile, opal-A forms when hydrothermal fluids become supersaturated and precipitate the silica from solution. The silica-rich, alkaline hydrothermal fluid cools within the range of 50-100 ºC and amorphous silica particles nucleate to form a colloidal suspension (Rimstidt and Cole, 1982). The colloids agglomerate and precipitates from solution produce cement, locally making sinter terraces (Rimstidt and Cole, 1982).

Cryogenic opal-A (COA) forms in hydrothermal systems that reach sub-zero air temperatures seasonally; such hydrothermal systems occur in Iceland and Yellowstone National Park (Channing and Butler, 2007; Jones and Renaut, 2010). COA forms when silica-rich hydrothermal fluid, which contains an alkali chloride (e.g., Na^+Cl^-), erupts sub-aerially and is exposed to sub-zero Celsius air temperatures (Channing & Butler, 2007; Fox-Powell et al., 2018). As the fluid cools, opal-A nucleates and precipitates in the same mechanism as sinter terraces. As the temperature falls below the freezing point of water, ice crystals start to form which removes the solvent and partitions dissolved salts and colloidal silica into brine veins (Channing & Butler, 2007). The brine veins in between forming ice crystals become super-saturated with respect to silica and high in ionic strength, which promotes silica nucleation, polymerization, and particle growth (Channing & Butler, 2007; Fox-Powell et al., 2018). When the COA-containing ice melts, unconsolidated COA particles are washed away from the location

of formation and are deposited downstream (Channing and Butler, 2007). COA takes the shape of the brine veins in which they form and are commonly tube- or funnel-shaped (Channing & Butler, 2007; Fox-Powell et al., 2018). Fox-Powell et al. (2018) found that synthetic COA can trap microorganisms and has the potential to preserve signs of biological activity.

It is plausible that COA exists on Mars because of the existence of ancient hydrothermal systems (Farmer, 1996) and sub-zero temperatures on Mars in the present and the past. Although COA has the potential to preserve signs of life, it is currently unknown how freezing temperature and initial solution chemistry affect the preservation process. Additionally, different freezing temperatures and solution chemistries may result in distinct silica morphologies, which may provide information about past climates and geochemical conditions on Mars. This has implications for the potential for past life, and is especially relevant considering that the future Mars 2020 mission will be selecting materials for a sample return mission. In this work, the effect of freezing temperatures (-20, -80, and -196 °C) and solution chemistry (chlorine and sulfur based solutions) on the morphology of resulting COA was investigated in order to determine if COA morphology can be used as an indicator for past climate and fluid chemistry.

1.1 Ancient hydrothermal systems on Mars

The motivation of this research was to determine if COA in future Mars return-samples could provide clues about past martian environmental conditions, although it is also applicable to terrestrial samples. The existence of COA on Mars requires that there were hydrothermal systems in the past. Ancient hydrothermal systems likely existed on Mars based on evidence from surface features and mineralogy (Farmer, 1996, and references therein). There are several types of geomorphic features on Mars that suggest ancient hydrothermal activity including channels along the margins of impact crater melt sheets, channels along ancient volcanic slopes,

volcanic fissures, fretted channel terraces, caldera floor features, and rifted basins (Farmer, 1996, and references therein). Allen and Oehler (2008) used multiple imagers and instruments on the Mars Reconnaissance Orbiter (MRO) to assess potential hydrothermal surface features in Vernal Crater, Arabia Terra, Mars. Surface characteristics observed in Vernal Crater including size, elliptical shape, color, terracing, and location of fractures were similar to analog spring deposits in the Dalhousie Complex, Australia (Allen and Oehler, 2008). Silica deposits in Gusev Crater have also been interpreted to be caused by hot springs (Ruff and Farmer, 2016). Additionally, silica in Syrtis Major has been proposed to have formed through high-temperature hydrothermal processes (Stok et al., 2010). Evidence from SNC meteorites show that magmatic activity occurred on Mars as late as 0.18 Ga (e.g., Nyquist et al., 2001).

1.2 Martian Climate

The existence of COA on Mars also requires that past surface temperatures were below the freezing temperature of water. Past climate on Mars is not fully understood, but there is evidence that supports a cold and dry climate compatible with COA formation (e.g., Fastook et al., 2012; Cannon et al., 2017) although some studies support the idea of a warm and wet ancient climate (Squyres and Kasting, 1994; Craddock and Howard, 2002). A cold ancient martian climate is supported by the interpretation that eskers exist in the south circumpolar region of Mars, which implies glaciation-related deposits near the Noachian-Hesperian boundary (Fastook et al., 2012). Glacial accumulation and ice-flow models by Fastook et al. (2012) showed that using typical Noachian-Hesperian geothermal heat fluxes, the mean annual south polar atmospheric temperature was between -75 and -50 ºC. This implies that low-latitude mean annual atmospheric temperatures were below the melting point of water-ice, although

temperatures could have exceeded the melting point of water-ice seasonally (Fastook et al., 2012). Additionally, despite the low atmospheric pressure, liquid water was stable on the surface of ancient Mars based on evidence of lake deposits and channels (e.g., Malin and Edgett, 2003; Grotzinger et al., 2015). The ~3.6 - 3.2 billion year old lake deposits being investigated by the *Curiosity* rover in Gale crater may have accumulated over ~10,000 to 10,000,000 years, and individual lakes in Gale Crater were likely stable on the surface for minimum durations ranging from 100 to 10,000 years (Grotzinger et al., 2015). Thus, the ancient climate and water stability on Mars suggest that COA could exist on the surface.

1.3 Opaline silica on Mars

Exposures of opaline silica have been detected by the Miniature Thermal Emission Spectrometer (mini-TES) at Columbia Hills of Gusev Crater, adjacent to the "Home Plate" feature. These features have been suggested to be the result of precipitation from hot springs or geysers, acid-sulfate leaching of basalts from fumarole steam condensates, and low-temperature acid weathering of bedrock (McAdam et al., 2008; Squyres et al., 2008; Ruff et al., 2011). Precipitation from a hot spring or geyser is supported by an undisturbed stratiform relationship with the underlying local rock and lack of cross-cutting or fracture controlled occurrences (Ruff et al., 2011). The resemblance of "Home Plate" opaline silica morphology to that of microbially mediated micro-stromatolites at the El Tatio hydrothermal system suggests that a biotic origin cannot be ruled out (Ruff and Farmer, 2016). Further studies into the formation of hydrothermal silica on Mars may help elucidate whether "Home Plate" silica could be biotically mediated or if it has the potential to trap signs of past life.

Another hypothesis by Squyres et al. (2008) stated that acid-sulfate steam condensates from fumaroles leached the metal cations from basalts, leaving amorphous silica near Home Plate.

This idea is supported by the presence of the immobile cation titanium in the amorphous silica (Squyres et al., 2008). Low-temperature acid weathering of local bedrock from an acid spring and/or surface release of solution has also been proposed as a formation mechanism of amorphous silica at Home Plate (McAdam et al., 2008). This hypothesis is supported by the localized nature of silica deposits, co-occurrence with TiO_2, and the occurrence of sulfates near and below the silica deposits (McAdam et al., 2008).

Opaline silica has also been detected in ancient and relatively young surface materials by orbital spectrometers (e.g., Milliken et al., 2008; Rapin et al., 2018). The Compact Reconnaissance Imaging Spectrometer for Mars (CRISM) instrument on board the Mars Reconnaissance Orbiter has detected H_2O and SiOH-bearing phases most consistent with opaline silica and glass in the plains surrounding Valles Marineris, (Milliken et al., 2008; Weitz et al., 2013). These deposits have been interpreted as either the result of low-temperature, acidic weathering of basaltic rocks or directly precipitated silica cement due to a lack of evidence of volcanic structures in the near vicinity (Milliken et al., 2008; Weitz et al., 2013). Hydrated silica has also been detected on the sides of a volcanic cone in the Syrtis Major Caldera complex by Stok et al. (2010). They suggested that this silica was formed by high temperature hydrothermal processes because of its proximity to distinct volcanic features.

In Gale Crater, instruments on the *Curiosity* rover have detected up to ~90 wt.% SiO_2 in Murray and Stimson Formation sedimentary rocks (Frydenvang et al., 2017; Rapin et al., 2018). The Chemistry and Mineralogy (CheMin) X-ray spectrometer (XRD) on board *Curiosity* analyzed the Buckskin sample from the Murray mudstone and showed a large amorphous component that consisted of opal-A or silica glass as well as opal-CT (Morris et al., 2016; Rampe et al., 2017). Additionally, laser induced breakdown spectroscopy (LIBS) of high-silica

rocks in the Murray and Stimson formations revealed that the silica was hydrated, with an average of 6.3 ± 1.4 wt.% water (Rapin et al., 2018). Laboratory experiments by Rapin et al. (2018) suggested that the hydration state of the silica is most consistent with opal-A. Opaline silica discovered in the Stimson and Murray formations have been hypothesized to have formed from diagenetic processes (e.g., Frydenvang et al., 2017; Rapin et al., 2018).

The potential return of samples cached by the Mars 2020 rover offers an opportunity to look for COA in returned samples from Mars. The detection of COA would indicate that opal-A formed through hydrothermal processes rather than fumarole-related weathering or low temperature acid-leaching of basalts. This is important for understanding the geologic history of the landing site, the history of hydrothermal systems on Mars, and past climate. By studying the formation mechanisms of COA in the laboratory and the effects of solution chemistry and freezing temperature on its morphology, we can prepare for the analysis and interpretation of silica-bearing samples returned from Mars.

1.4 Factors controlling opal-A precipitation on Earth

Precipitation of opal-A in hydrothermal systems on Earth, called “sinter”, is controlled by evaporation, temperature, pH, dissolved salts, and cation effects (Marshall and Warakomski, 1980; Guidry and Chafetz, 2002). Dissolved cations can affect silica solubility and catalyze its precipitation (Ichikuni, 1970; Rimstidt and Cole, 1983). Dissolved cations including aluminum and iron have been shown to decrease the solubility of silica and result in chemically impure precipitates (Ickikuni, 1970). Additionally, the solubility of amorphous silica is dependent on the type of dissolved salt (Marshall and Warakomski, 1980). Marshall and Warakomski (1980) tested the effect of several salts on the solubility of amorphous silica and demonstrated that silica solubility decreases with increasing salt concentration. Out of the salts tested, $MgCl_2$ and $CaCl_2$

decreased the silica solubility the most and $NaHCO_3$ the least (Marshall and Warakomski, 1980). At 25 °C, silica was approximately 1.25 times more soluble in a Na_2SO_4 solution than in a NaCl solution of the same concentration (Marshall and Warakomski, 1980).

pH is also known to have an effect on silica solubility, although studies are less conclusive (Siever, 1962; Marshall and Warkomski, 1980; Guidry and Chafetz, 2002). Alexander et al. (1941) demonstrated that silica solubility is fairly constant from pH 2 to 9.5, above which the solubility increases due to ionization of H_4SiO_4. This effect has also been demonstrated in silica/salt (Na_2SO_4 and NaCl) solutions, where the silica solubility rapidly increases above pH ~9 (Marshall and Warkomski, 1980). However, the effect of pH on silica solubility is unclear in natural systems. In natural hydrothermal systems in Steamboat Springs, Nevada, there was no clear relationship between pH and the degree of supersaturation of silica (White et al., 1956).

Temperature also has a major effect on the solubility of amorphous silica (Siever, 1962). Amorphous silica solubility is approximately 800 ppm at 200 °C compared to approximately 200 ppm at 50 °C (Siever, 1962, and references therein). Temperature was shown to be the most significant driver of silica solubility in two hot springs at Yellowstone National Park (Guidry and Chafetz, 2002). Hinman and Lindstron (1996) attributed precipitation of hydrothermal opal-A to cooling of hot spring water when it comes in contact with cooler air temperatures. They also attributed enhanced silica precipitation in winter months to cooler water temperatures.

In this study, temperature, pH, and dissolved salts were variables in inducing the precipitation of opal-A. Two different acids (HCl and H_2SO_4) and three freezing temperatures were used to precipitate COA. Additionally, the acids served to lower the pH to circum-neutral, thus decreasing the silica solubility even more. The variables that affect silica solubility (namely

temperature and dissolved salts) are hypothesized to affect the timing and morphology of resulting COA.

2 Materials and Methods

Two Earth and Mars relevant solutions were prepared by dissolving sodium metasilicate (Sigma Aldrich, CAS: 6834-92-0) in 18.2 MΩ water using the methods described by Channing and Butler (2007). Hydrochloric acid (HCl; CAS 7647-01-0) and sulfuric acid (H_2SO_4; CAS 7664-93-9) solutions were used to titrate the sodium metasilicate solutions to a circum-neutral pH of approximately 7.5, producing dissolved silica and salt (reactions 1 and 2) (Table 1).

$$2Na^+ + SiO_3^{-2} \cdot 5H^+ + 5OH^- + 2H^+ + 2Cl^- \rightarrow 2Na^+ + 2Cl^- + SiO_2 + 6H^+ + 6OH^- \quad (1)$$

$$2Na^+ + SiO_3^{-2} \cdot 5H^+ + 5OH^- + 2H^+ + SO_4^{-2} \rightarrow 2Na^+ + SO_4^{-2} + SiO_2 + 6H^+ + 6OH^- \quad (2)$$

HCl was chosen because it is plausible based on the chemistry of natural geothermal fluids at Yellowstone National Park, where natural COA has been found (Channing and Butler, 2007) (Table 1). Hydrothermal systems in El Tatio, Chile are also chorine dominated (Table 1). There is also an abundance of chlorinated species on Mars, including chlorides, chlorates, and perchlorates (e.g., Ruuesch et al., 2012; Elsenousy et al., 2015; Sutter et al., 2017; Hogancamp et al., 2018). H_2SO_4 was chosen because on Mars, silica-rich hydrothermal solutions can be acidified through oxidation of sulfides in the country rock, producing $SiO_2^-{}_{(aq)}$ and $SO_4^-{}_{(aq)}$ (McAdam et al., 2008), and the discovery of jarosite at multiple landing sites suggests the presence of acid-sulfate fluids on ancient Mars (e.g., Squyres et al., 2004; Rampe et al., 2017). Sub-samples of the starting solutions (sodium metasilicate and hydrochloric acid or sulfuric acid) were taken before heating. Additionally, the resulting dissolved salts (Na_2SO_4 and NaCl) are

known to have different effects on silica solubility and are therefore ideal for testing the role of solution chemistry on COA morphology (Marshall and Warkomski, 1980).

The silica/salt solutions were heated to 50 °C to simulate hydrothermal temperatures while being agitated with a magnetic stir bar. Once the solution reached 50 °C, it was poured into several 50 mL plastic centrifuge tubes and sealed. The tubes were either flash frozen in liquid nitrogen (-196 °C) or frozen overnight in -20 °C or -80 °C freezers. The frozen solutions were thawed at room temperature until a cloudy suspension was observed at the bottom of each tube. A plastic pipette was used to remove the silica suspension from the tube and place it on a SEM stub with carbon tape. The SEM stub was air dried, gently washed with 18.2 MΩ water to remove salts, and air dried again. This method was used to avoid breaking apart delicate COA particles but also remove salts, and is interpreted as the best way to obtain in-tact COA particles for traditional SEM methods. The samples were carbon coated and analyzed with a JEOL 5910LV scanning electron microscope (SEM) with an energy dispersive spectroscopy (EDS) component at the NASA Johnson Space Center. A beam energy of 15 kV and working distance of 20 mm was used. EDS measurements were taken with a SiLi detector with a thin window and with a voltage of 10 keV for 60 seconds in order to achieve >3000 counts. iXRD iridium software was used to process EDS data.

The remainder of the silica suspension was vacuum filtered through 0.22 μm filter paper, following the method of Channing and Butler (2007). The white precipitate was washed with 18.2 MΩ water to remove salt and then dried at room temperature. The silica precipitate was disaggregated using an agate mortar and pestle and then analyzed by X-ray diffraction (XRD) using a PANalytical X'Pert Pro MPD X-ray Diffraction Spectrometer with Co Kα radiation (λ= 1.78901 Å) at the Johnson Space Center. Data were collected every 0.02 degrees 2θ at 40 mA

and 45kV from 4 to 80 degrees 2θ with a step size of 0.02˚. XRD patterns were overlaid using the MDI Jade software to compare and confirm the presence of X-ray amorphous material.

Opal-A was also formed through evaporation in order to compare the morphology with COA. The same starting solutions (sodium metasilicate with sulfuric acid or hydrochloric acid) were heated to 50 ºC, and then placed in a glass beaker in a 50 °C oven overnight to evaporate water. The precipitate was washed with 18.2 MΩ water and vacuum filtrated with 0.22 um filter paper to remove salts. The precipitate was then dried and placed on an SEM stub for imaging.

The sub-samples of the starting solutions (sodium metasilicate and hydrochloric acid or sulfuric acid) that were taken before heating were analyzed using ion chromatography (IC) for their chloride and sulfate concentrations (Table 1). These initial ionic compositions were used in the Fortran-based modeling program, FREZCHEM 15.1, to model the possible precipitated minerals of freezing silica/hydrochloric acid and silica/sulfuric acid solutions. FREZCHEM is a chemical thermodynamic model that is unique in that it models concentrated electrolyte solutions at temperature below 0 ℃ based on the Pitzer model (Marion, 2008). Any resulting geochemical models using silica should be viewed with the caveat that the silica parameters in FREZCHEM database are not based on experimental data below 0 °C (Marion et al., 2011). However, FREZCHEM theoretical calculations are equivalent to independent silica experimental measurements that validate the model (Marion et al., 2011). In addition, Geochemist's Workbench (GWB) was utilized to affirm the minerals precipitated via FREZCHEM at 0 ºC. The saturation indices of silica and salts were modeled in GWB through evaporation as water was removed from the system.

Table 1. pH and chemical compositions of natural and synthetic hydrothermal solutions.

Solution	pH at measurement	$SiO_2^{-}_{(aq)}$ (ppm)	$Na^{+}_{(aq)}$ (ppm)	$Cl^{-}_{(aq)}$ (ppm)	$SO_4^{-}_{(aq)}$ (ppm)
Yellowstone-Minute Geyser [1]	7.6	450	380	610	28
El Tatio-geyser [2]	7.3	205	4345	7899	42.9
Synthetic hydrothermal fluid [3]	6.5	450	unknown	unknown	0
Synthetic hydrothermal solution A (this study)	7.5	450	169.8	889 ± 25.2	0
Synthetic hydrothermal solution B (this study)	7.5	450	169.8	0	1170 ± 26.0

3 Results

3.1 X-ray diffraction of COA

Amorphous materials, such as opal-A, are characterized by a broad "hump" in XRD patterns due to a lack of long-range crystallographic order. XRD analyses confirmed that all COA material was largely amorphous in nature and resembled an opal-A reference material (Figure 1). XRD patterns of the synthesized COA material did not resemble an opal-CT reference pattern because of broader amorphous "humps" (Figure 1). XRD patterns of COA peaked at slightly higher angles than the reference opal-A material, indicating slightly lower SiO_2 polymerization.

[1] (Nordstrom et al., 2005)
[2] (Cortecci et al., 2005)
[3] (Channing and Butler, 2007; Fox-Powell et al., 2018)

XRD results indicated that there was no salt contamination in the synthesized COA samples within the instrumental detection limit. Additionally, the same COA material that was analyzed in the XRD was analyzed using SEM. There was no evidence of salt contamination in SEM images of the COA material that was analyzed with XRD.

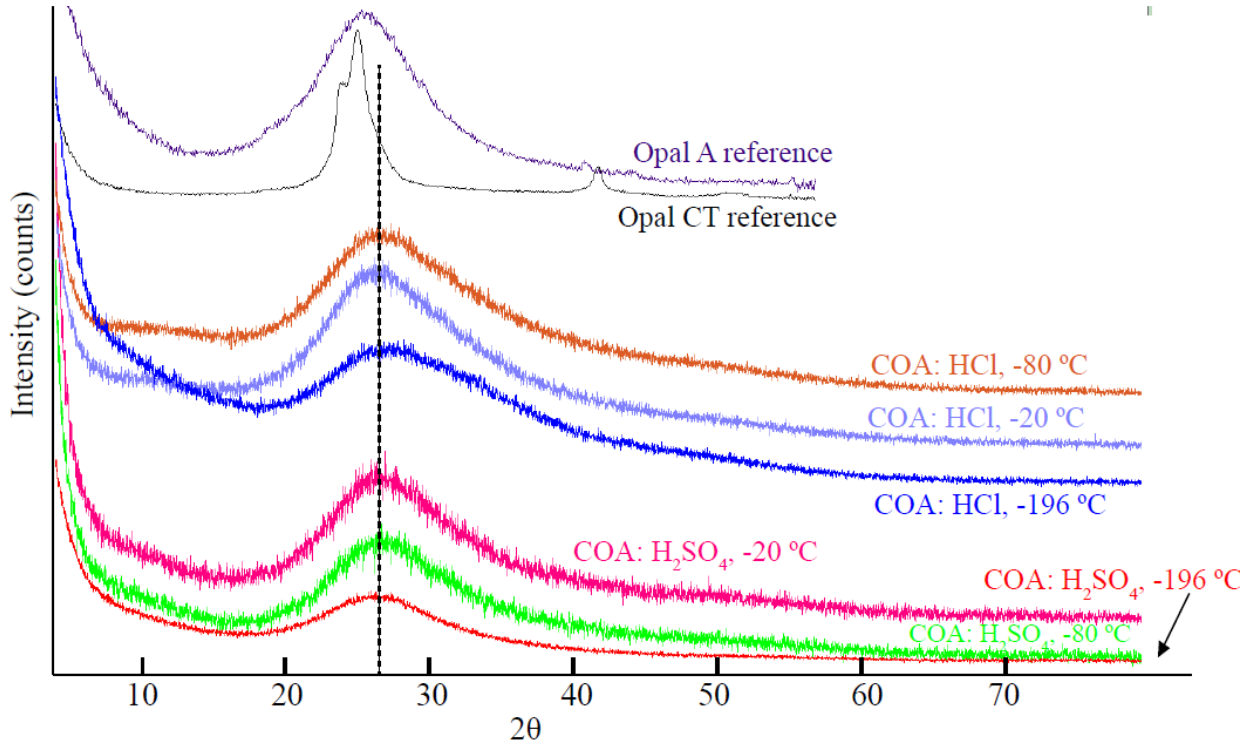

Figure 1. XRD patterns of COA powders overlaid with an opal-A and opal-CT reference material. Patterns were shifted up or down on the y-axis so that individual patterns were distinguishable. Dashed vertical line represents the peak maximum for the opal-A reference material, which peaks at 26° 2θ and 4.03 Å. (2 column figure)

3.2 COA synthesized with HCl

Morphological analyses of COA materials consisted of looking at several SEM images and making measurements of randomly selected COA particles. Although several SEM images

were taken from each sample, typical examples are presented in this paper so that qualitative differences are apparent. The morphology of COA made in HCl solutions generally consisted of smooth, branch-like particles that decreased in size with decreasing freezing temperature. COA made at -20 °C produced smooth silica branches and funnels with widths ranging from approximately 8-25 µm (Figure 2). The silica funnels observed are characterized by an elongate silica particle with a curving inward end (Figure 2a). Silica branches can be several hundred microns in length and were commonly fragmented into smaller pieces due to drying or sample preparations (Figure 2b). Many of the silica branches were cemented onto silica plates, which were also fragmented (Figures 2c-d). Desiccation cracks with sub-micron widths were observed (Figure 3a-b). EDS confirmed that all the material was composed of Si and O, and had no measureable Na or Cl contamination.

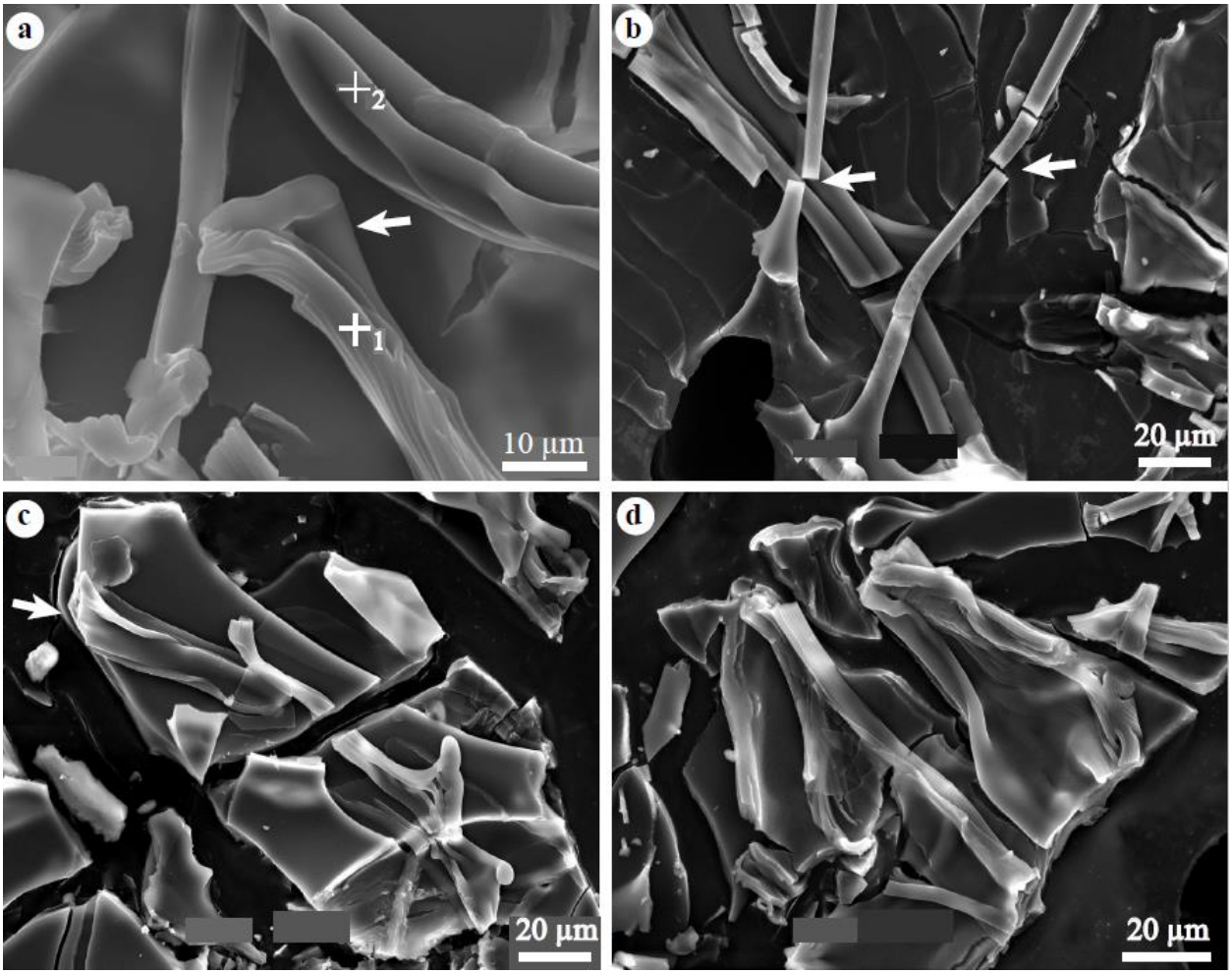

Figure 2. SEM images of COA prepared using a starting solution of silica and hydrochloric acid. The solution was heated to 50 ºC and then frozen overnight in a -20 ºC freezer. The white arrows point to funnel-shaped silica in (a), which EDS confirmed were made of Si and O in spots 1 and 2. Smooth, elongate branches (b) were fragmented into smaller pieces (white arrows). Funnels on silica plates (c and d) were also observed. (2 column figure)

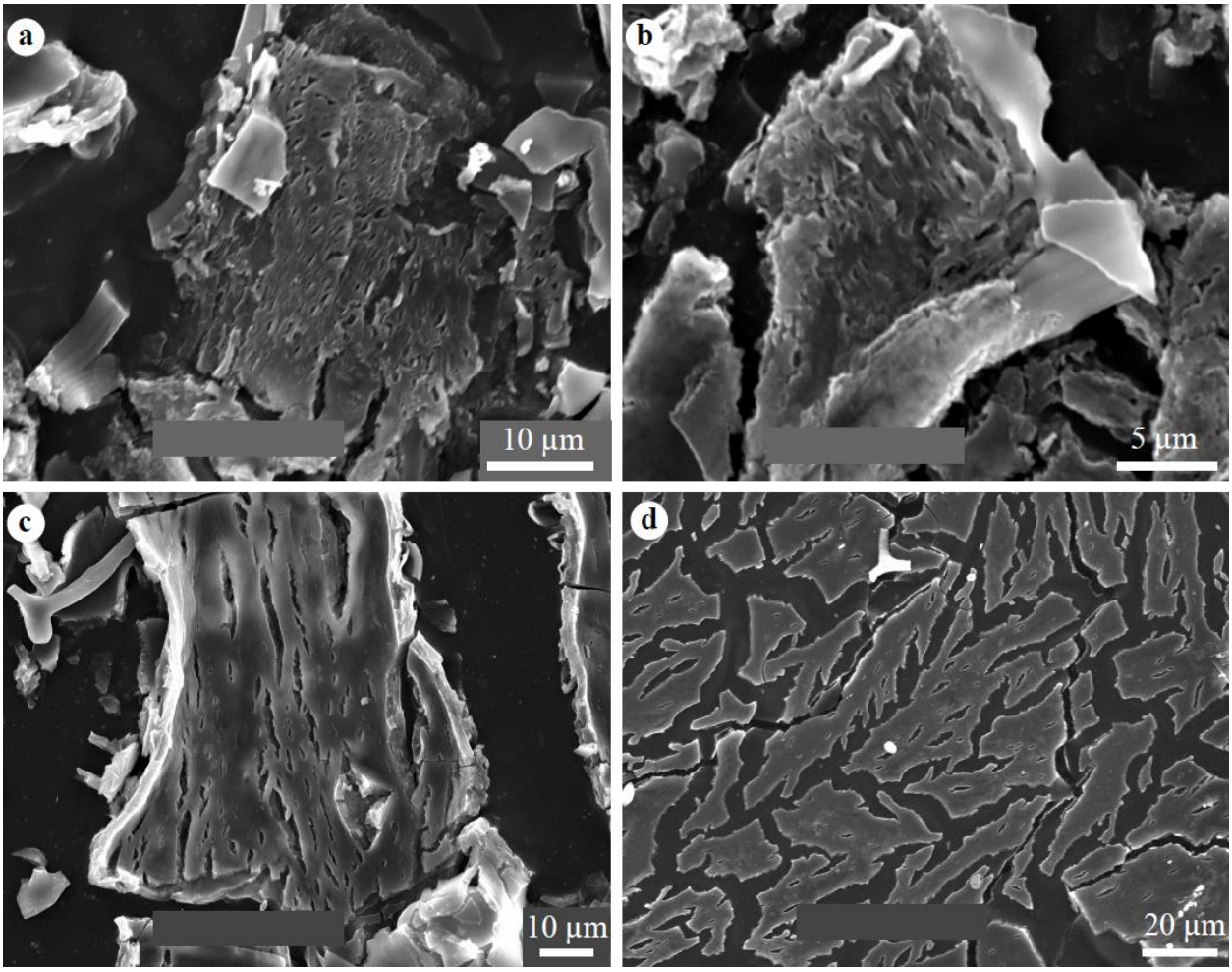

Figure 3. SEM images of desiccation cracks observed in COA prepared using a starting solution of silica and hydrochloric acid, heated to 50 ºC and then frozen overnight in a -20 ºC freezer (a and b) and in a -80 ºC freezer (c and d). (2 column figure)

COA made at -80 °C also produced smooth silica branches and funnels with widths ranging from approximately 4-20 µm (Figure 4). Several silica pieces with triple junction geometry (Figure 4a-b) were observed. Additionally, several silica pieces contained halite dendrites precipitated within them as seen in the COA particle cross-section (Figure 4c-d). Desiccation cracks with widths ranging from sub-micron to 2 µm were observed (Figure 3c-d).

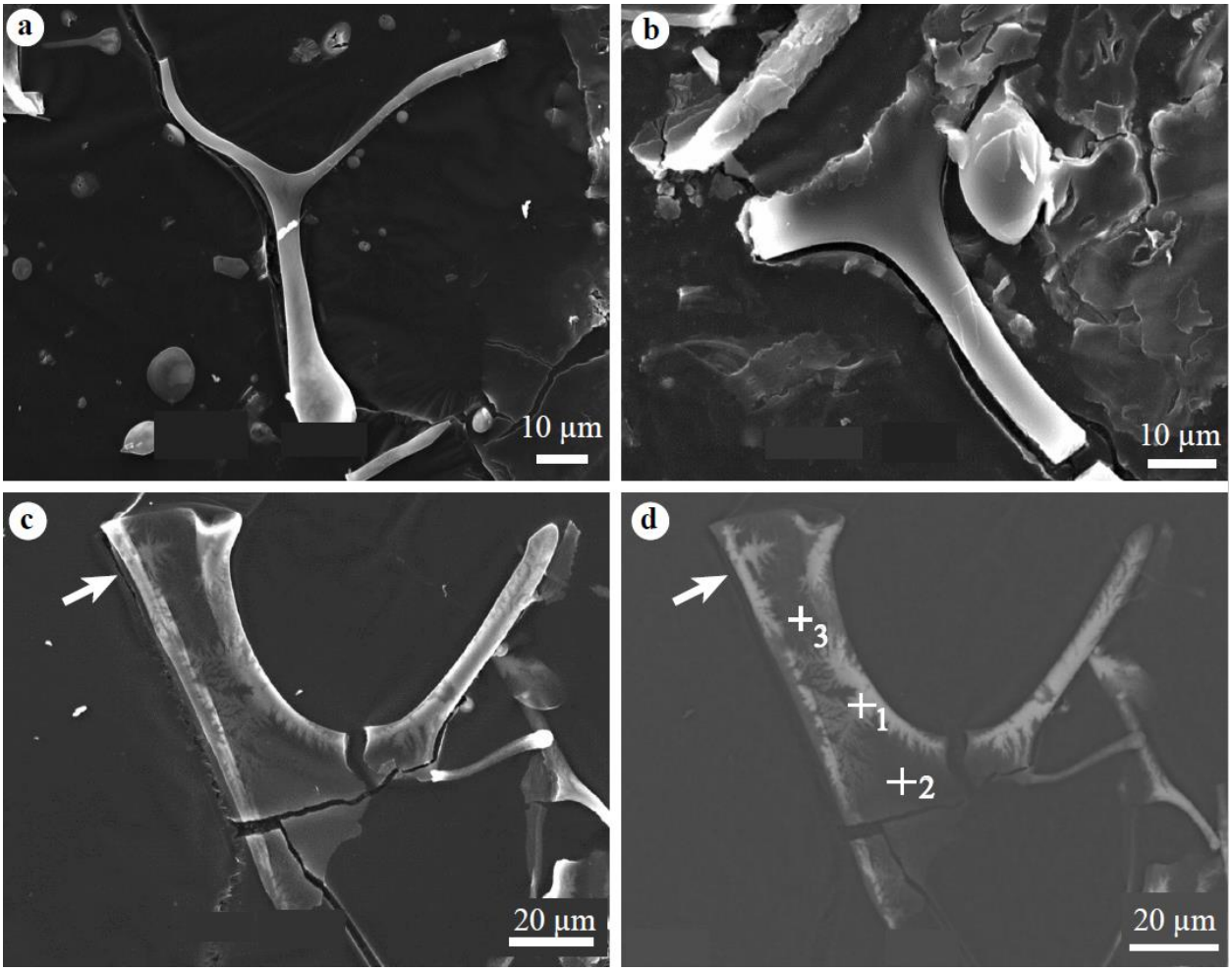

Figure 4. SEM images of COA prepared using a starting solution of silica and hydrochloric acid. The solution was heated to 50 ºC and then frozen overnight in a -80 ºC freezer. SEM images show smooth silica pieces with triple junction geometry (a and b). Funnel-shaped silica with halite dendrites embedded within it was observed (c and d). EDS confirmed that spot 1 (d) contained Na and Cl, whereas spots 2 and 3 contained Si and O. The white arrows point out the embedded halite within the silica funnels. (2 column figure)

COA made at -196 °C was primarily composed of complex, multi-directional silica ropes with widths ranging from approximately <1-3 µm (Figure 5a-b). These silica ropes were curved and interconnected. Multiple irregularly shaped pores with diameters ranging from sub-micron

to 2 µm were observed in generally flat silica pieces (Figure 5c-d). Larger pores with irregular boundaries (average diameter of 2 µm) were surrounded by many smaller pores (diameters < 1 µm). EDS confirmed that all particles were composed of Si and O.

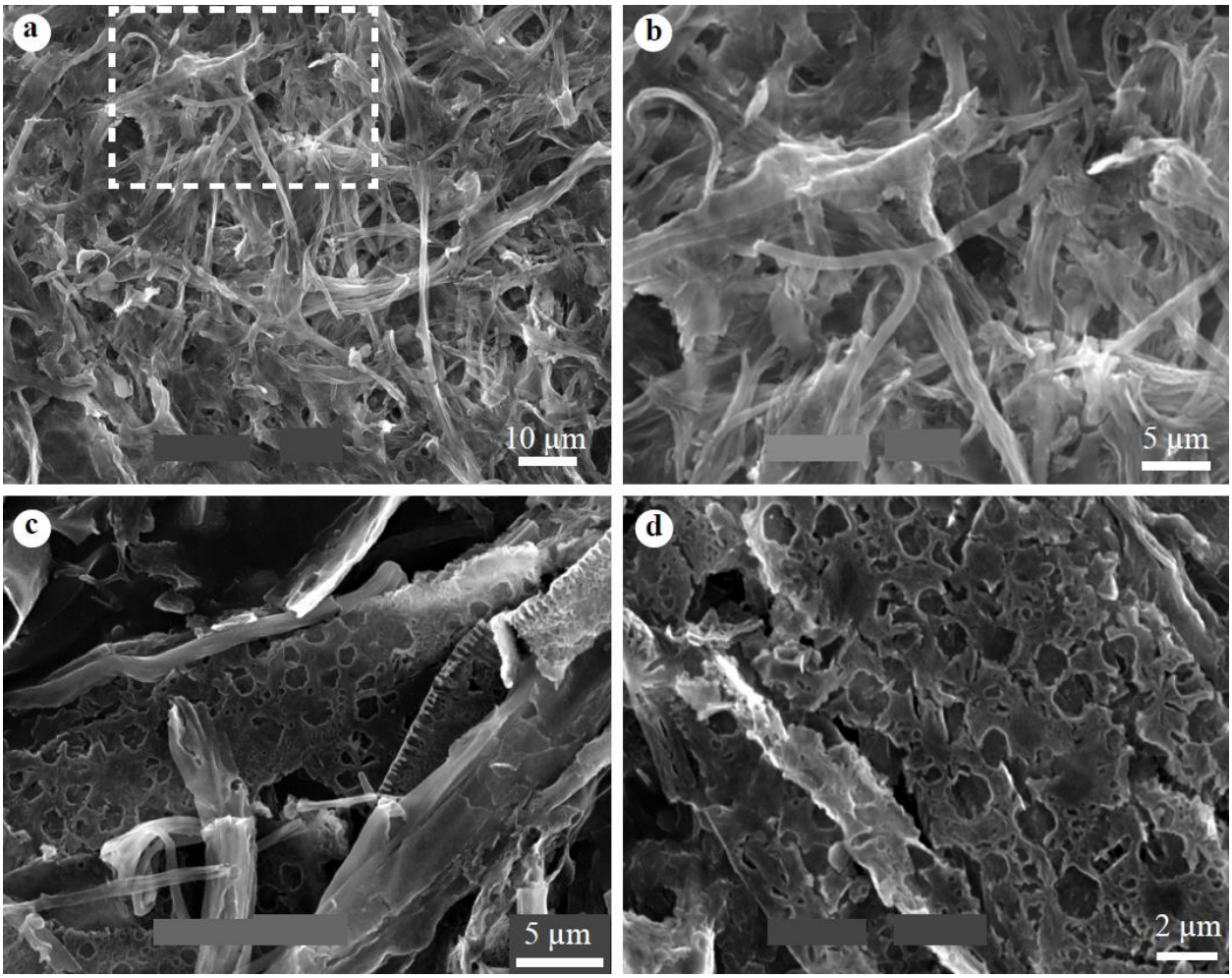

Figure 5. SEM images of COA prepared using a starting solution of silica and hydrochloric acid. The solution was heated to 50 ºC and then flash frozen using liquid nitrogen (-196 ºC). SEM images showed complex silica ropes with branch widths ranging from approximately <1-3 µm (a). (b) is a zoomed in image of the white dashed box shown in (a), showing the complex silica branches in more detail. Irregular pores with diameters ranging from sub-micron to 2 µm were observed (c and d). (2 column figure)

Opal-A made with hydrochloric acid and then precipitated through evaporation did not display the tube-like, ropey morphology that is unique to COA. Opal-A particles synthesized through evaporation were irregular in shape but had flat surfaces (Figure 6).

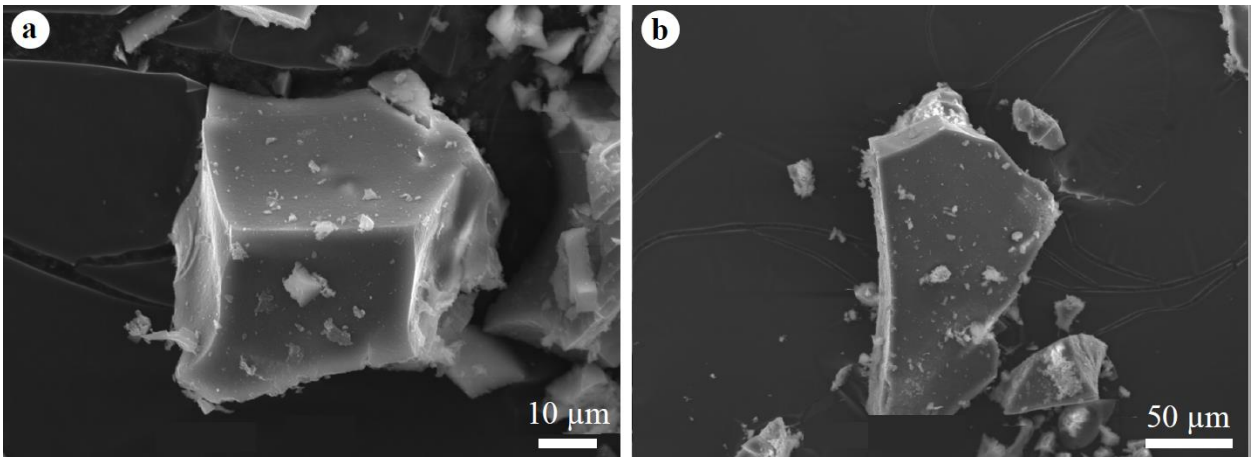

Figure 6. Opal-A made with hydrochloric acid (a-b) by evaporating solutions at 50 ºC overnight. (2 column figure)

3.3 COA made using H_2SO_4

COA made by adding H_2SO_4 to a sodium silicate solution produced jagged, fragmented silica that decreased in size with decreasing freezing temperature. COA made at -20 °C produced jagged silica "hash" with no systematic structure (Figure 7). Many of the silica pieces contained round holes with diameters ranging from 5 to 10 µm, some of which were fragmented in half (Figure 7). Particle size varied from sub-micron to approximately 25 µm.

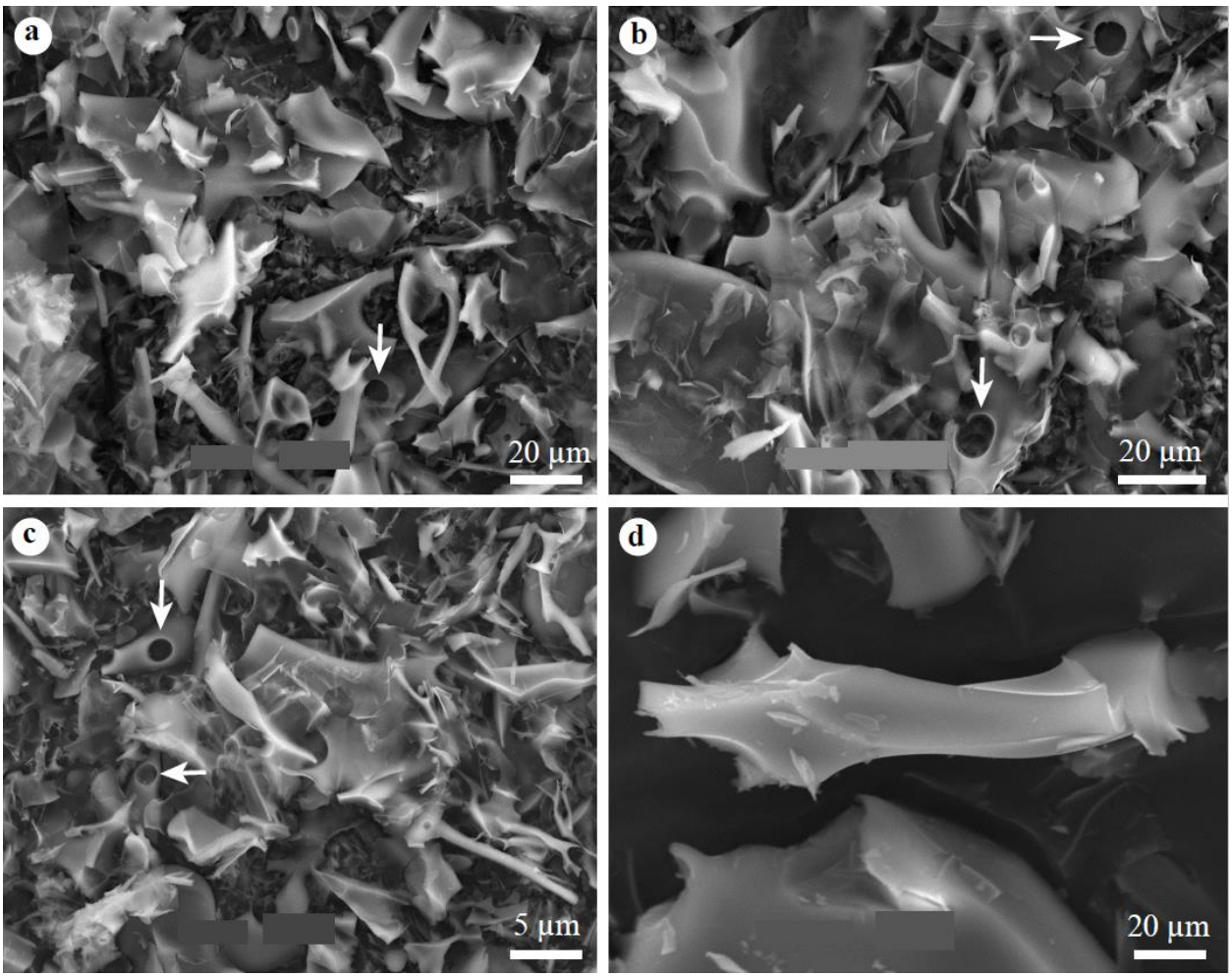

Figure 7. SEM images of COA prepared using a starting solution of silica and sulfuric acid. The solution was heated to 50 ºC and then frozen overnight in a -80 ºC freezer. Silica pieces are jagged, fragmented, and contain ~10 µm circular holes (some are indicated with white arrows). Individual silica pieces were angular (d). (2 column figure)

COA particles made at -80 °C were similar in shape and texture to COA made at -20 °C, but were slightly smaller in size, with widths ranging from sub-micron to approximately 15 µm (Figure 8). The silica pieces contained many circular holes with diameters ranging from 5 to 10 µm (Figure 8). The COA also displayed complex braiding patterns due to desiccation, with each individual "braid" having a width of approximately 1 µm (Figure 8c-d).

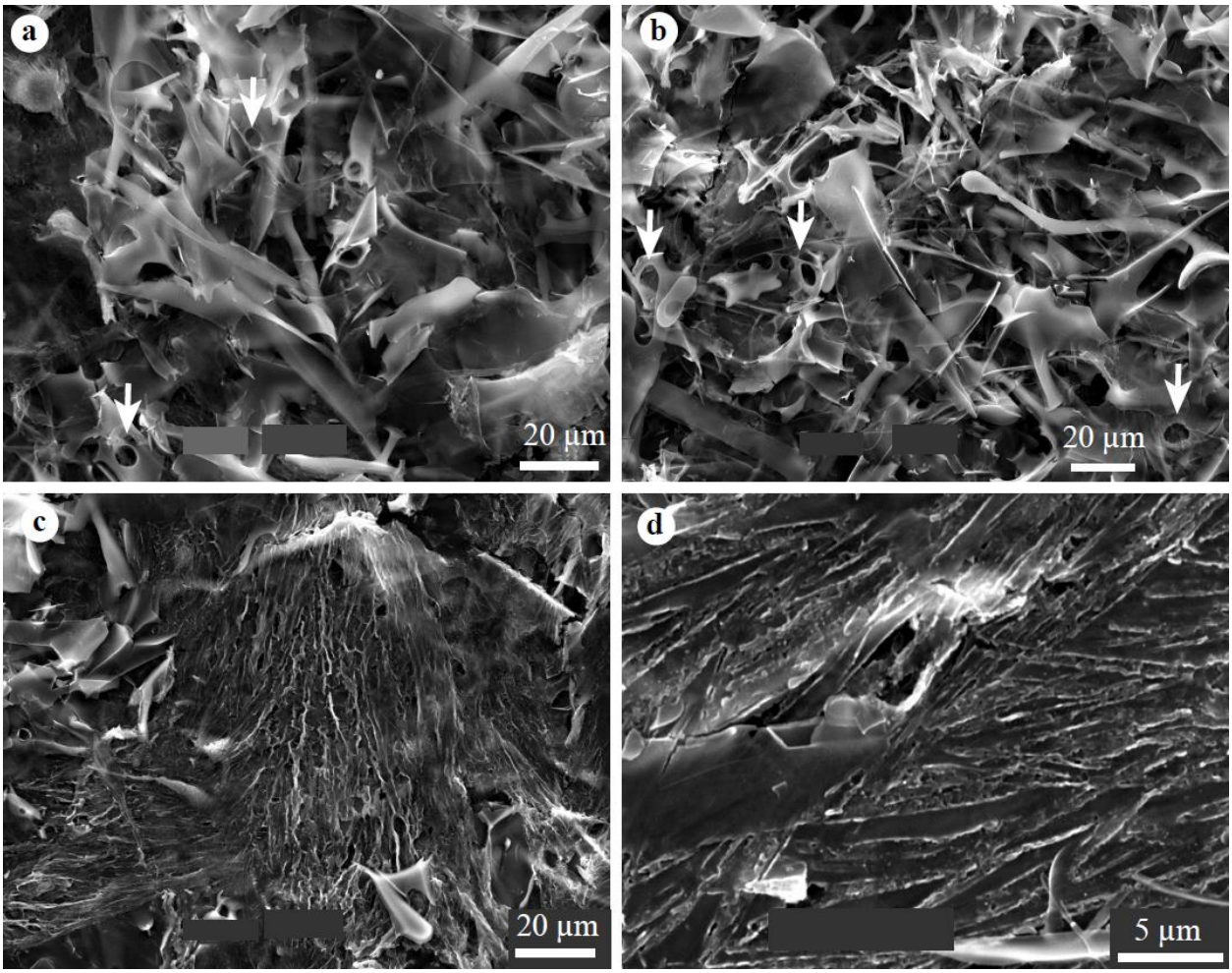

Figure 8. SEM images of COA prepared using a starting solution of silica and sulfuric acid. The solution was heated to 50 ºC and then frozen overnight in a -80 ºC freezer. Images show jagged, fragmented silica pieces with ~10 µm holes (some are indicated with white arrows) (a and b). Jagged, linear patterns due to desiccation were also observed (c and d). (2 column figure)

COA made at -196 °C consisted of complex, multi-directional, angular silica pieces with widths ranging from sub-micron to 2 µm (Figure 9). The COA made at -196 °C was much smaller than the COA made at -20 and -80 °C. Multiple circular pores with diameters of less than 1 µm were observed in the COA (Figure 9d).

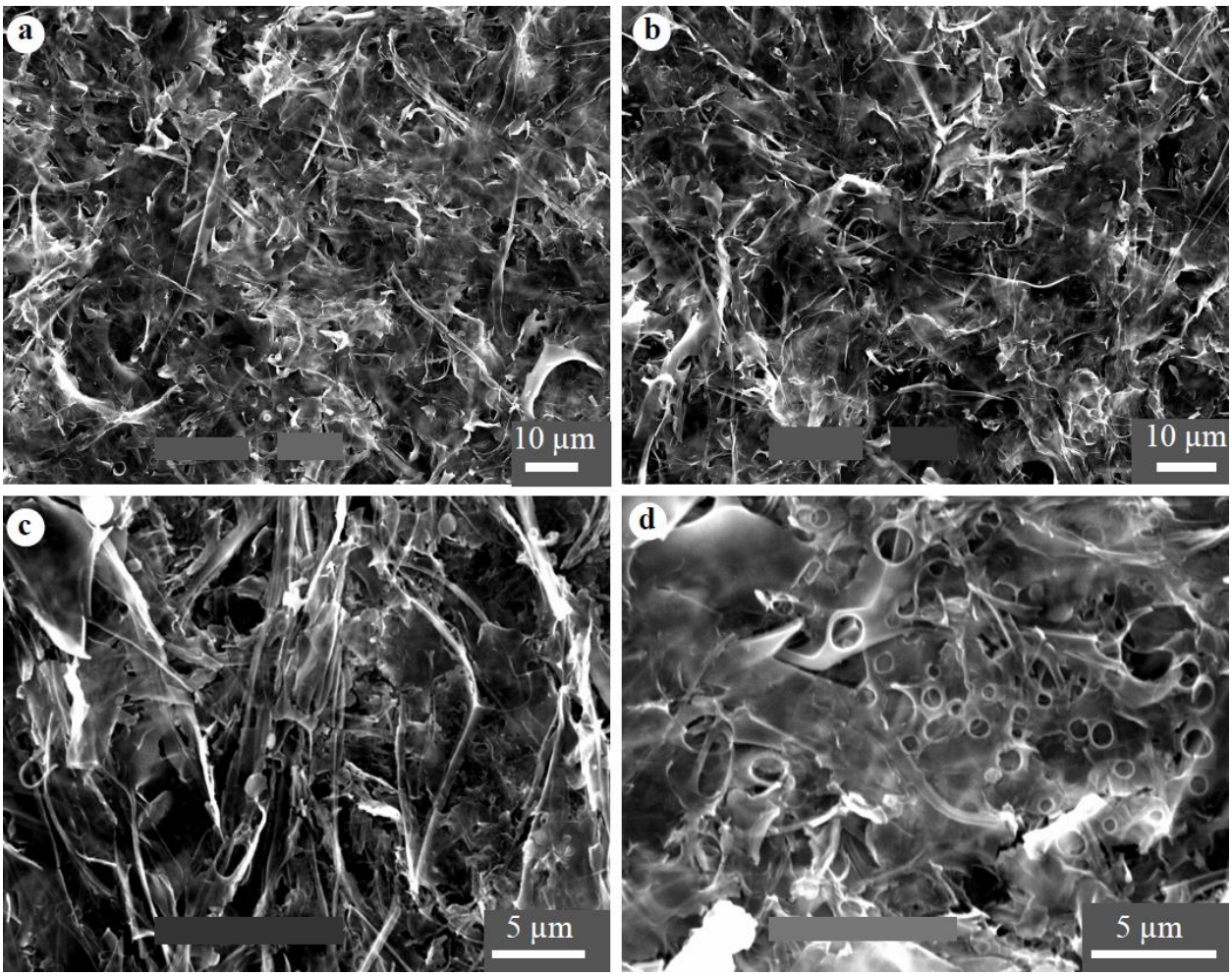

Figure 9. SEM images of COA prepared using a starting solution of silica and sulfuric acid. The solution was heated to 50 ºC and then flash frozen using liquid nitrogen (-196 ºC). Silica pieces are jagged, fragmented, and contain pores with diameters ranging from sub-micron to 2 µm (d). (2 column figure)

The morphology of opal-A made with sulfuric acid and then precipitated through evaporation was generally similar to that of opal-A made with hydrochloric acid (Figures 6, 10). However, there was an abundance of irregularly shaped silica pieces with a jagged, rough texture in the silica precipitated from sulfuric acid solutions (Figure 10). EDS confirmed that all the particles imaged using SEM were composed of Si and O, and contained no salt contamination.

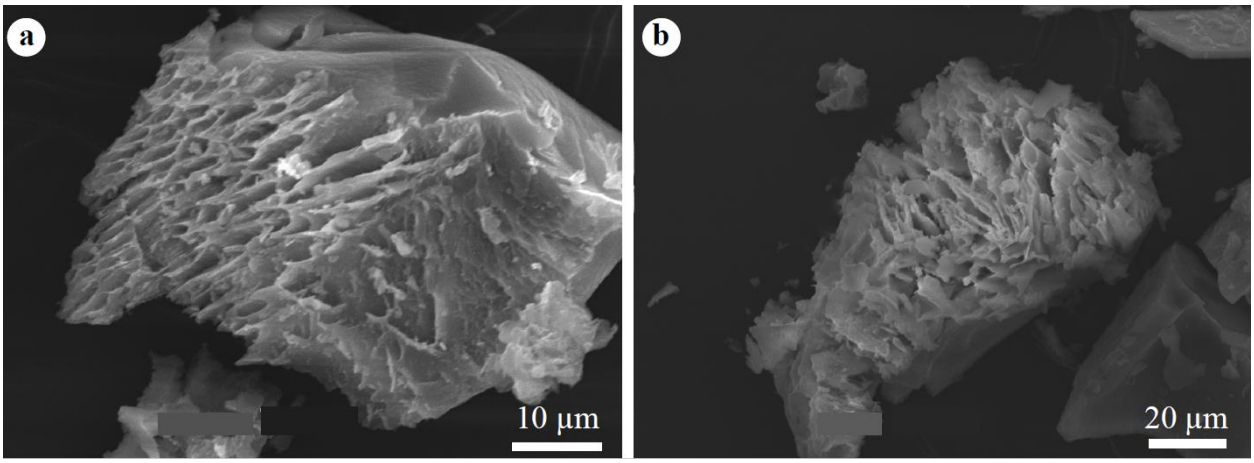

Figure 10. Opal-A made with sulfuric acid (a-b) by evaporating solutions at 50 ºC overnight. (2 column figure)

4 Discussion

4.1 Effect of freezing temperature on morphology

The rate of ice crystal growth in a cooling solution influences the purity of the ice (i.e., how much solute is incorporated into the ice structure) (Hasan and Louhi-Kultanen, 2015). High freezing rates, which leads to faster ice crystal growth, does not allow enough time for the solute to effectively diffuse away from the advancing ice crystal front (Hasan and Louhi-Kultanen, 2015). COA that was flash frozen at -196 °C had small particle sizes because dissolved silica and salt were trapped within ice. COA made at -20 and -80 °C exhibited larger particle sizes because the silica and salt solutes had more time to diffuse away from the growing ice front and concentrate in larger brine veins.

The morphologies of the synthetic COA material were also compared to opal-A precipitated through evaporation in order to show the differences between cryogenic and non-cryogenic opal-A synthesized in this lab using two different solution chemistries. The unique morphologies observed in COA (Figures 2-5, 7-9) are due to cryogenic processes and are not

observed in opal-A made by evaporation (Figure 6, 10), which agrees with previous studies by Channing and Butler (2007). Ice crystals that surround brine veins serve as molds for COA growth and form unique opal-A morphologies such as tubes and funnels (Channing and Butler, 2010). These morphologies are not observed in opal-A made without freezing because of the absence of ice crystals during precipitation. Opal A precipitated through evaporation also appears similar in texture to smooth opal-A from a core drilled through a hot-spring deposit at Yellowstone National Park, Wyoming (Guidry and Chafetz, 2003).

4.2 Effect of solution chemistry on morphology

The size and shape of ice crystals formed during cooling are affected significantly by cooling rate but are also affected by the type of solute (Petzold and Aguilera, 2009). The morphologies of the ice crystals and/or salts in the synthetic hydrothermal solution are important because they serve as the mold for the COA particles. Additionally, the type(s) of solute affects the solubility of silica. At 25 °C, dissolved NaCl decreases the amorphous silica solubility greater than dissolved Na_2SO_4 (Marshall and Warakomski, 1980). If this relationship holds true below the 25 °C, silica would start to precipitate at a higher temperature in the hydrochloric acid solutions than in the sulfuric acid solutions. Additionally, the solubility of sodium chloride and sulfate may affect the morphology of resulting COA. At 0 °C, sodium chloride is approximately 7 times more soluble than sodium sulfate (Bharmoria et al., 2012; Bharmoria et al., 2014).

FREZCHEM models using the initial concentrations of Na^+, Cl^-, and SiO_2 (Table 1) demonstrated that theoretically, SiO_2 should precipitate before $NaCl \cdot 2H_2O$ (Figure 11). The FREZCHEM model, although it has its limitations, suggests that silica and ice formed, followed by $NaCl \cdot H_2O$ (Figures 11, 12). Sodium chloride, which tends to form at interfaces rather than in

solution (Rodriguez-Navarro and Doehne, 1999), precipitated around the silica in the brine veins (Figure 12). When the ice melted and the salts were washed away, smooth, tubular COA particles remained.

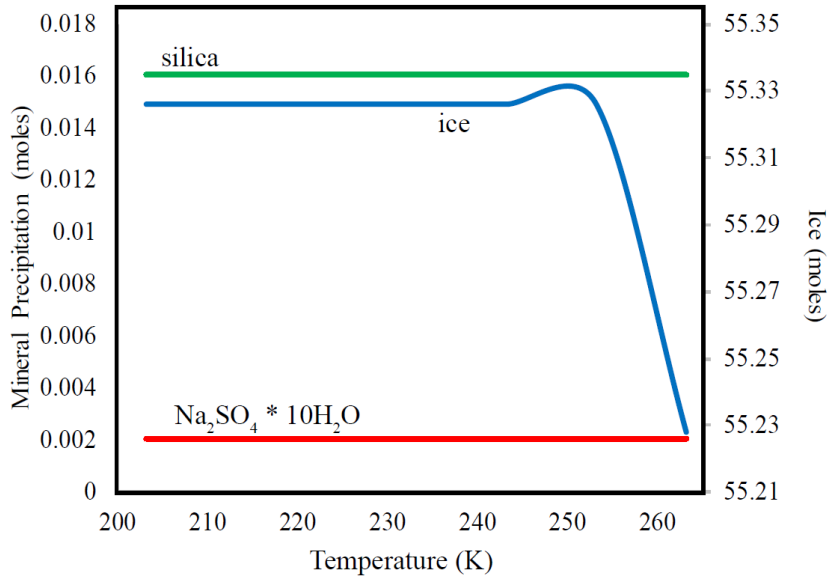

Figure 11. FREZCHEM geochemical model showing water-ice formation and mineral precipitation during freezing of the HCl/silica solution over a range of 200-255 K. This temperature range was chosen in order to force the precipitation of hydrated salts in FREZCHEM. (1 column figure)

COA formed using sulfuric acid solutions resulted in angular, fragmented silica particles, indicating that the silica precipitated within an angular mold and/or that salts grew into the COA (Figures 7-9). The angularity of COA made with sulfuric acid solutions may be explained by a combination of two scenarios:

1) COA formed in brine veins and then sulfate salts precipitated around it, causing an increase in crystallization pressure and growth of sulfate salts into COA (Figure 12). Salt-weathering studies

have found that sodium sulfate growth is more damaging to porous rocks than sodium chloride (Rodriguez-Navarro and Doehne, 1999). Salt weathering is caused when a salt crystallizes in a confirmed volume such as a pore. The build-up of crystallization pressure against the surrounding material causes growth into the surrounding material. This scenario would result in fragmented, angular COA particles and is supported by GWB geochemical modeling, which suggests that the majority of silica precipitates before sulfate salts at low temperatures (Figure 13). Additionally, evaporation was simulated in GWB because FREZCHEM could not be used to show temperature of mineral precipitation of mirabilite and silica. The GWB databases do not extend below 0 °C, therefore evaporation was used as a proxy for liquid-water removal. GWB evaporation modeling showed that at 0 °C, the saturation index of amorphous silica and quartz was higher than mirabilite until ~0.08 kg liquid water remained, at which the saturation index of mirabilite exceeded amorphous silica (Figure 13). This supports the idea that most COA precipitated within brine veins prior to sulfate salt precipitation.

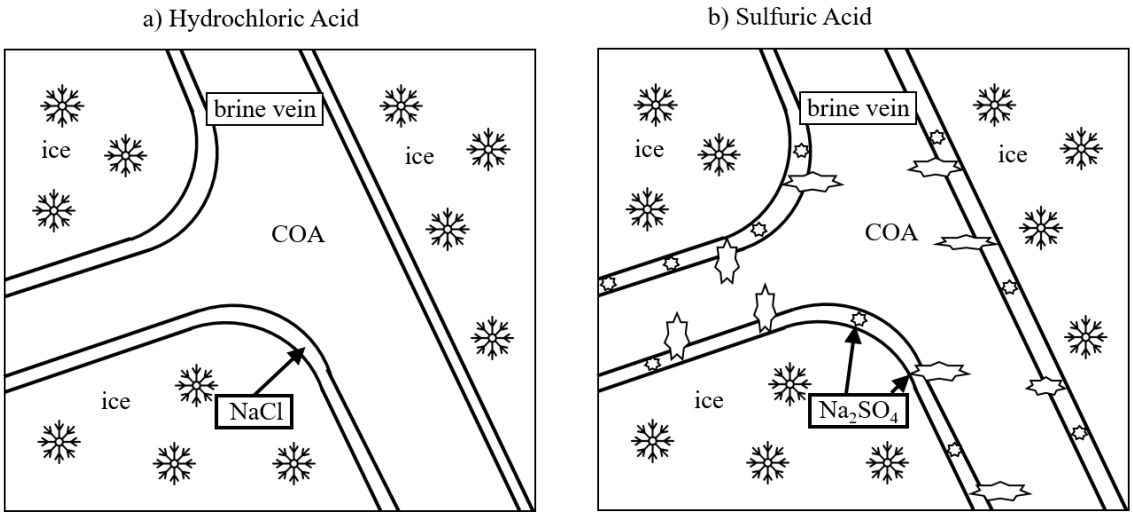

Figure 12. Morphology of COA resulting from synthetic hydrothermal solutions made with a) hydrochloric acid and b) sulfuric acid. (2 column figure)

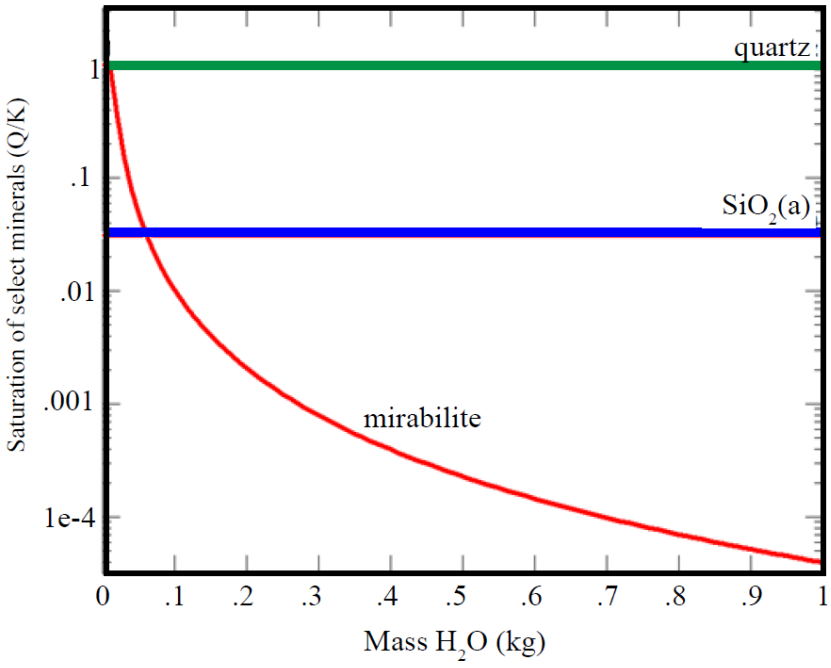

Figure 13. Geochemist's Workbench geochemical modeling showing mineral saturation of amorphous silica (SiO_2(a)), mirabilite, and quartz at 0 °C as water is removed via evaporation. (1 column figure)

2) Sulfate salts precipitated in the remaining liquid brine, as depicted in Figure 12. In this scenario, the sulfate crystals formed in the brine veins through subfluoresence (Rodriguez-Navarro and Doehne, 1999) and any remaining silica in solution precipitated around it. When the sulfate was washed away during the melting of ice, the silica that precipitated in the brine broke apart into angular pieces. Although geochemical modeling suggests that most sulfate salts precipitated before silica (Figure 13), there may have been some silica co-precipitating with sulfate salts.

All COA particles made with sodium sulfate were characterized by well-rounded holes with diameters ranging from <1 µm-10 µm within the silica (Figures 7-9). These holes were interpreted to be caused by a liquid within the precipitating silica because they are equidimensional and lack irregular boundaries that would be consistent with corrosion or solid phase growth. The liquid was likely concentrated H_2SO_4 because there was excess sulfate in the starting solution relative to sodium (Table 1) and H_2SO_4 has an extremely low freezing point. The freezing point of H_2SO_4 is as low as ~-66 °C at 37 wt.% H_2SO_4 and as high as ~8 °C at 100 wt.% H_2SO_4 (Ohtake, 1993). As water-ice started to form and silica and sulfate precipitated, there was still H_2SO_4 in the brine veins. It is important to note that these holes may not form in starting solutions without excess sulfate. The holes observed in COA are a clear indicator that the starting solution was sulfur based and not chlorine based, and that the amount of sulfate in solution exceeded the amount of cations (e.g., Na^+).

COA formed using chloride solutions resulted in tube, or rope-shaped silica particles (Figures 2, 4-5). These ropey, elongate particles indicate that they formed within brine channels between forming ice crystals. As the synthetic hydrothermal solution cooled, silica precipitated by the same method that silica sinters are formed. As the temperature fell below the freezing point of water, ice crystals formed first, then silica precipitated in the brine channels between the ice crystals because of the increasing ionic strength of the solution (Figure 10). After silica precipitated, it is likely that halite formed, but was then washed away when the ice melted. Many COA particles made with HCl solutions exhibited triple junction geometry (Figure 4), which is caused by the formation of silica at the intersection of three brine veins, such as those produced in experimental studies by Mader (1992). Silica funnels (Figures 2a, 4c) may form when silica forms around an ice or brine vein.

COA made with HCl solutions also contained halite dendrites within the COA structure (Figures 4c-d). This may be due in part to freezing rate, but also relates to the type of solute since the dendrites were only seen in COA made with HCl. Halite tends to form at interfaces rather than in solution (Rodriguez-Navarro and Doehne, 1999). Halite growing on the outsides of silica may apply a crystallization pressure that causes the halite to grow into the silica structure. Additionally, the halite may precipitate while silica is still a gel (in between the liquid and solid phase) and more easily grow into the silica structure rather than around it.

The irregularly shaped holes observed in COA made with an HCl solution at -196 °C (Figure 5) are interpreted to be "corrosion pits". Chen et al. (2017) observed pits similar to those observed in COA made with HCl at -196 °C, and attributed them to acid corrosion. Chen et al. (2017) found that corrosion pits with diameters ranging from a few microns to approximately 12 µm formed in high silica enamels (SiO_2 ranging from 54.62 to 64.62 wt %) with short term exposure to sulfuric acid. The corrosion pits formed in areas where the silica network was relatively loose in structure. These weak spots in silica experienced faster ion exchange, hydration, and hydrolysis reactions and resulted in shallow pits with depths of less than 10 µm (Chen et al., 2017). Corrosion pits were not observed in COA made with sulfuric acid solutions.

COA formed at -80 °C and -20 °C using HCl solutions also resulted in desiccation cracks (Figure 3). Micro-desiccation cracks in amorphous silica have not been reported in the literature, but are the result of air drying the silica suspension. Amorphous silica consists of Si tetrahedrally bound to oxygen atoms, which are covalently bound to hydroxyl groups called "bound water" (Lowen and Broge, 1961). In high relative humidity environments, water molecules can hydrogen bond to the silanol groups, making a layer of adsorbed water (Lowen and Broge, 1961). Desiccation occurs when the adsorbed water attached to the silanol groups evaporates and

causes the silica volume to decrease. Amorphous silica does not have a preferred crystal structure; therefore, the desiccation cracks are irregular in shape. Observance of these micro-desiccation cracks in returned samples from Mars would indicate periods of wetting, or higher humidity, and subsequent drying.

4.3 Comparison to natural and synthesized COA samples

Hydrothermal systems in Yellowstone National Park, Wyoming, and in Iceland contain chlorine-dominated fluids and reach air temperatures below 0 ºC seasonally (Table 1). COA collected from these locations are expected to have similar morphologies as the synthetic COA made with HCl solutions and frozen at -20 ºC in this study. Channing and Butler (2007) presented natural COA particles from Yellowstone National Park with tube, funnel, and triple-junction morphology similar to the COA materials in this study precipitated from HCl solutions at -20 °C. Similar morphologies were also observed in natural COA material from Iceland (Jones and Renaut, 2010).

Additionally, features in hydrothermal opal-A which have been attributed to bacteria need to be interpreted with caution based on the results from this work. The holes observed in COA made with sulfuric acid solutions are similar in size and shape to holes in terrestrial hydrothermal opal-A that have been attributed to bacterial fossils (Gepner et al., 2005, pp. 518; Jones and Renaut, 2010, pp. 26). The observation of these well-rounded micro-pores in abiotically synthesized opal-A samples is important for interpreting whether similar features in natural samples are abiotically or biotically formed.

The COA materials synthesized using HCl solutions at -20 ºC also resembled synthetic COA precipitated using the same conditions in different laboratories. Fox-Powell et al. (2018) synthesized COA with triple-junction morphology and delicate lattice structures that were the

same approximate size as the COA made under the same conditions in this study. Channing and Butler (2007) also precipitated COA with triple-junction morphology, tube, and funnels similar to COA made in this study using the same conditions. Overall, the morphology of COA made at -20 °C using HCl solutions is similar to the COA materials synthesized in different laboratories.

4.3 Implications for Earth and Mars climate and fluid chemistries

The results from this research represent COA morphologies that could result from simple, terrestrial and/or Mars-like solutions and freezing temperatures. It is clear that sulfur-dominated systems and chlorine-dominated systems produce COA with different morphologies. SEM analyses of COA in future Mars return samples may provide clues about past martian climate and fluid chemistry. COA morphologies can also be used to understand past Earth climate in areas where hydrothermal systems existed. Additionally, features observed in these abiotically synthesized COA materials resemble features attributed to bacterial fossils in natural hydrothermal opal-A samples (Gepner et al., 2005). Therefore, features observed in COA is also important when interpreting micro-features that have a potential biotic origin.

Regardless of microbe and organic material, the morphology of COA can indicate past climatic and geochemical conditions on Mars and Earth. Jagged, angular COA particles indicate a sulfur dominated systems whereas smooth, rope-like COA particles indicate a chloride dominated system. Holes in COA with diameters ranging from approximately 5 to 10 μm indicate that the initial hydrothermal solution was sulfur dominated. Additionally, the presence of micro-desiccation cracks indicate the drying of amorphous silica either by a reduction in pressure, increase in temperature, or decrease in relative humidity. The particle size of well-preserved COA particles can also provide information about past climate because smaller COA

particles are associated with colder freezing temperatures. COA morphology has the potential to contribute to the debate about whether ancient Mars was “cold and dry” or “wet and warm”.

Although COA particles are delicate and break apart into smaller pieces (Figure 2b), COA is preserved in young sediment deposits on Earth (Channing and Butler, 2007) and may be preserved in hot spring deposits on Mars, especially considering the minimal amount of surface weathering processes compared to Earth. COA particles in sedimentary deposits in Yellowstone National Park, Wyoming, and Geysir, Iceland, although fragmented, preserve morphologies (e.g., triple junction geometry, tubes, funnels) that are unique to their starting solution chemistries and freezing temperatures (Channing and Butler, 2007; Jones and Renaut, 2010). It is plausible that COA particles, although fragmented, would be preserved well enough to provide clues about initial solution chemistry and climate.

5 Conclusions

COA was formed using two terrestrial and Mars like solutions (sulfuric acid and hydrochloric acid) and three freezing temperatures (-20 °C, -80 °C, and -196 °C). SEM revealed that the morphology of COA is highly dependent on freezing temperature and initial solution chemistry. COA made with sulfuric acid solutions produced jagged, angular, and fragmented silica pieces with holes with diameters ranging from sub-micron to 10 μm. COA made with hydrochloric acid solutions formed smoother, rope-like particles. COA formed at lower freezing temperature, particularly -196 °C, produced complex silica pieces with very small particle sizes. The morphology of COA has implications for terrestrial samples as well as future sample return samples from Mars because it can elucidate past geochemical and climatic conditions. The ability of COA to trap organic particles may also depend on initial solution chemistry and

612 freezing temperature, and should be investigated further. Samples that have the potential to
613 contain COA should be highly considered for return samples in the upcoming Mars 2020 mission
614 because of their potential to infer information about past climate and geochemical conditions.

615 **Acknowledgments, Samples, and Data**

616 We thank Liz Rampe, Valerie Tu, and Doug Ming for their help with editing the manuscript.
617 All data are provided in the figures and tables within this manuscript.

618 **Funding**

619 Partial support for this research came from NASA Solar Systems Workings award number
620 80NSSC18K0333 to T.J. Lapen.

621 **References**

622 Alexander, G.B., Heston, W.M., Iler, R.K. (1954). The solubility of amorphous silica in water.
623 *Journal of Physical Chemistry*. 58, 453-455.

624

625 Allen, C.C. & Oehler, D.Z. (2008). A case of ancient spring in Arabia Terra, Mars. *Astrobiology*.
626 8, 1093-1112, doi:10.1089/ast.2008.0239.

627

628 Bharmoria, P., Gehlot, P.S., Gupta, H., Kumar, A. (2014). Temperature-dependent solubility
629 transition of Na_2SO_4 in water and the effect of NaCl therein: solution structures and salt water
630 dynamics. *The Journal of Physical Chemistry*. 118, 12734-12742, doi: 10.1021/jp507949h.

631

632 Bharmoria, P., Gupta, H., Mohandas, V.P., Ghosh, P.K., Kumar, A. (2012). Temperature
633 invariance of NaCl solubility in water: inferences from salt-water cluster behavior of NaCl, KCl,
634 and NH_4Cl. *The Journal of Physical Chemistry*. 116, 11712-11719, doi: 10.1021/jp307261g.
635
636 Cannon, K.M., Parman, S.W., Mustard, J.F. (2017). Primordial clays on Mars formed beneath a
637 steam of supercritical atmosphere. *Nature*. 552, 88-91, doi: 10.1038/nature24657.
638
639 Channing, A., & Butler, I.B. (2007). Cryogenic opal-A deposition from Yellowstone hot springs.
640 *Earth and Planetary Science Letters*. 257, 121-131.
641
642 Chen, X., Chafetz, H.S., Andreasen, R., Lapen, T.J. (2017). Silicon isotope compositions of
643 euhedral authigenic quartz crystals: implications for abiotic fractionation at surface temperatures.
644 *Chemical Geology*. 423, 61-73.
645
646 Cortecci, G., Boschetti, T., Mussi, M., Herrera, L., Mucchino, C., Barbieri, M. (2005). New
647 chemical and original isotopic data on waters from El Tatio geothermal field, northern Chile.
648 *Geochemical Journal*. 39, 547-571.
649
650 Craddock, R.A. & Howard, A.D. (2002). The case for rainfall on a warm, wet early Mars.
651 *Journal of Geophysical Research: Planets*. 107, 1-36, doi: 10.1029/2001JE001505.
652

Elsenousy, A., Hanley, J., Chevier, V.F. (2015). Effect of evaporation and freezing on the salt paraagenesis and habitability of brines at the Phoenix landing site. *Earth and Planetary Science Letters*. 421, 39-46, doi: 10.1016/j.epsl.2015.03.047.

Farmer, J.D. (1996). Hydrothermal systems on Mars: an assessment of present evidence, *Ciba Found Symposium*. 202, 195-299.

Fastook, J.L., Head, J.W., Marchant, D.R., Forget, F., Madeleine, J. (2012). Early Mars climate near the Noachian-Hesperian boundary: independent evidence for cold conditions from basal melting of the south polar ice sheets (Dorsa Argentea Formation) and implications for valley network formation. *Icarus*. 219, 25-40, doi: 10.1016/j.icarus.2012.02.013.

Fox-Powell, M.G., Channing, A., Applin, D., Mann, P., Cloutis, E., Preston, L.J., Cousins, C.R. (2018). Cryogenic silicification of microorganisms in hydrothermal fluids. *Earth and Planetary Science Letters*. 498, 1-8, https://doi.org/10.1016/j.epsl.2018.06.026.

Frydenvang, J., Gasda, P. J., Hurowitz, J. A., Grotzinger, J. P., Wiens, R. C., Newsom, H. E., Edgett, K.S., Watkins, J., Bridges, J.C., Maurice, S., Fisk, M.R., Johnson, J.R., Rapin, W., Stein, N.T., Clegg, S.M., Schwenzer, S.P., Bedford, C.C., Edwards, P., Mangold, N., Cousin, A., Anderson, R.B., Payre, V., Vaniman, D., Blake, D.F., Lanza, N.L., Gupta, S., Van Beek, J., Sautter, V., Meslin, P.Y., Rice, M., Milliken, R., Gellert, R., Thompson, L., Clark, B.C., Sumner, D.Y., Fraeman, A.A., Kinch, K.M., Madsen, M.B., Mitrofanov, I.G., Jun, I., Calef, F., Vasavada,

675 A.R. (2017). Diagenetic silica enrichment and late-stage groundwater activity in Gale crater,
676 Mars. *Geophysical Research Letters*. 44, 4716-4724.
677
678 Gepner, A.R., Ivanovskaya, T.A., Pokrovskaya, E.V. (2005). Hydrothermal fossilization of
679 microorganisms at the Earth's surface in Iceland. *Lithology and Mineral Resources*. 40, 505-520.
680
681 Grotzinger, J.P., Gupta, S., Malin, M.C., Rubin, D.M., Schieber, J., Siebach, K., Sumner, D.Y.,
682 Stack, K.M., Vasavada, A.R., Arvidson, R.E., Calef III, F., Edgar, L., Fischer, W.F., Grant, J.A.,
683 Griffes, J., Kah, L.C., Lamb, M.P., Lewis, K.W., Mangold, N., Minitti, M.E., Palucis, M., Rice,
684 M., Williams, R.M.E., Yingst, R.A., Blake, D., Blaney, D., Conrad, P., Crisp, J., Dietrich, W.E.,
685 Dromart, G., Edgett, K.S., Ewing, R.C., Gellert, R., Hurowitz, J.A., Kocurek, G., Mahaffy, P.,
686 McBride, M.J., McLennan, S.M., Mischna, M., Ming, D., Milliken, R., Newsom, H., Oehler, D.,
687 Parker, T.J., Vaniman, D., Wiens, R.C., Wilson, S.A. (2015). Deposition, exhumation, and
688 paleoclimate of an ancient lake deposit, Gale Crater, Mars. *Science*. 350, doi:
689 10.1126/science.aac7575.
690
691 Guidry, S.A. & Chafetz, H.S. (2003). Depositional facies and diagenetic alteration in a relict
692 siliceous hot-spring accumulation: examples from Yellowstone National Park, U.S.A. *Journal of*
693 *Sedimentary Research.* 73, 806-823, doi: 10.1306/022803730806.
694
695 Hasan. M. and Louhi-Kultanen, M. (2015). Ice growth kinetics modeling of air-cooled layer
696 crystallization from sodium sulfate solutions. *Chemical Engineering Science*. 133, 44-53, doi:
697 10.1016/j.ces.2015.01.050.

Hinman, N. & Lindstrom, R. (1996). Seasonal changes in silica deposition in hot spring systems. *Chemical Geology*. 132, 237-246.

Hogancamp, J.V., Sutter, B., Morris, R.V., Archer, P.D., Ming, D.W., Rampe, E.B., Mahaffy, P., Navarro-Gonzalez, R. (2018). Chlorate/Fe-bearing phase mixtures as a possible source of oxygen and chlorine detected by the Sample Analysis at Mars (SAM) instrument in Gale Crater, Mars. *Journal of Geophysical Research: Planets*. 123, 2920-2938, doi: 10.1029/2018JE005691.

Ichikuni, M. (1970). Incorporation of aluminum and iron into siliceous sinters. *Chemical Geology*. 6, 273-279.

Jones, B. & Renaut, R.W. (2010). Impact of seasonal changes on the formation and accumulation of soft siliceous sediments on the discharge apron of Geysir, Iceland. *Journal of Sedimentary Research*. 80, 17-35.

Lowen, W.K. & Broge, E.C. (1961). Effects of dehydration and chemisorbed materials on the surface properties of amorphous silica. *Journal of Physical Chemistry*. 65, 16-19, doi: 10.1021/j100819a006.

Mader, H. (1992). Observations of the water-vein systems in polycrystalline ice. *Journal of Glaciology*. 38, 333-347.

721 Malin, M. C., & Edgett, K. S. (2003). Evidence for persistent flow and aqueous sedimentation on
722 early Mars. *Science.* 302, 1931-1934.
723
724 Marion, G.M., Catling, D.C., Crowley, J.K., Kargel, J.S. (2011). Modeling hot spring chemistries
725 with applications to martian silica formation. *Icarus*. 212, 629-642. doi:
726 10.1016/j.icarus.2011.01.035.
727
728 Marion, G. M. & Kargel, J. S. (2008). Cold aqueous planetary geochemistry with FREZCHEM:
729 From modeling to the search for life at the limits. Berlin. Springer.
730
731 Marshall, W.L. & Warakomski, J.M. (1980). Amorphous silica solubility II. Effect of aqueous
732 salt solutions at 25 °C. *Geochimica et Cosmochimica Acta*. 44, 915-924.
733
734 McAdam, A.C., Zolotov, M.Y., Mironenko, M.V., Sharp, T.G. (2008). Formation of silica by
735 low-temperature acid alteration of martian rocks: physical-chemical constraints. *Journal of*
736 *Geophysical Research: Planets.* 113, doi: 10.1029/2007JE003056.
737
738 Milliken, R.E., Swayze, G.A., Arvidson, R.E., Bishop, J.L., Clark, R.N., Ehlmann, B.L., Green,
739 R.O., Grotzinger, J.P., Morris, R.V., Murchie, S.L., Mustard, J.F., Weitz, C. (2008). Opaline
740 silica in young deposits on Mars. *Geology*. 36, 847-850, doi: 10.1130/G24967A.1.
741
742 Morris, R. V., Vaniman, D. T., Blake, D. F., Gellert, R., Chipera, S. J., Rampe, E. B., Ming,
743 D.W., Morrison, S.M., Downs, R.T., Treiman, A.H., Yen, A.S., Grotzinger, J.P., Achilles, C.N.,

744 Bristow, T.F., Crisp, J.A., Des Marais, D.J., Farmer, J.D., Fendrich, K.V., Frydenvang, J., Graff,
745 T.G., Morookian, J., Stolper, E.M., Schwenzer, S.P. (2016). Silicic volcanism on Mars evidenced
746 by tridymite in high-SiO_2 sedimentary rock at Gale crater. *Proceedings of the National Academy*
747 *of Sciences of the United States of America*. 113, 7071–7076, doi:10.1073/pnas.1607098113.
748
749 Nordstrom, D.K., Ball, J.W., McCleskey, B. (2005). Ground water to surface water: chemistry of
750 thermal outflows in Yellowstone National Park. *Geothermal Biology and Geochemisty and*
751 *Yellowstone National Park*. 74-94.
752
753 Nyquist, L. E., Bogard, D.D., Shih, C.-Y., Greshake, A., Stoffler, D., Eugster, O. (2001). Ages
754 and geologic histories of the Martian meteorites. *Space Science Reviews.* 96, 105– 164.
755
756 Ohtake, T. (1993). Freezing points of H_2SO_4 aqueous solutions and formation of stratospheric ice
757 clouds. *Tellus*. 45, 138-144.
758
759 Petzold, G. & Aguilera, J.M. (2009). Ice morphology: fundamentals and technological
760 applications in food. *Food Biophysics*. 4, 378-396, doi: 10.1007/s11483-009-9136-5.
761
762 Pitzer, K. (1991). Ion interaction approach: Theory and data correlation. *Activity Coefficients in*
763 *Electrolyte Solutions*. 2, 75-153.
764
765 Rampe, E. B., Ming, D. W., Blake, D. F., Bristow, T. F., Chipera, S. J., Grotzinger, J. P., Morris,
766 R.V., Morrison, S.M., Vaniman, D.T., Yen. A.S., Achilles, C.N., Craig, P.I., Des Marais, D.J.,

Downs, R.T., Farmer, J.D., Fendrich, K.V., Hazen, R.M., Kah, L.C., Morookian, J.M., Peretyazhko, T.S., Sarrazin, P., Treiman, A.H., Berger, J.A., Eigenbrode, J., Fairen, A.G., Forni, O., Gupta, S., Hurowitz, J.A., Lanza, N.L., Schmidt, M.E., Siebach, K., Sutter, B., Thompson, L.M. (2017). Mineralogy of an ancient lacustrine mudstone succession from the Murray formation, Gale crater, Mars. *Earth and Planetary Science Letters*. 471, 172–185, doi: 10.1016/j.epsl.2017.04.021.

Rapin, W., Chauvire, B., Gabriel, T.S., McAdam, A.C., Ehlmann, B.L., Hardgrove, C., Meslin, P.Y., Rondeau, B., Dehouck, E., Franz, H.B., Mangold, N., Chipera, S.J., Wiens, R.C., Frydenvang, J., Schroder, S. (2018). In Situ Analysis of Opal in Gale Crater, Mars. *Journal of Geophysical Research: Planets*. 123, 1955-1972, doi: 10.1029/2017JE005483.

Rimstidt, J.D. & Cole, D.R. (1982). Geothermal Mineralization I: The mechanism of formation of the Beowawe, Nevada siliceous sinter deposit. *American Journal of Science*. 283, 861-875, doi:10.2475/ajs.283.8.861.

Rodriguez-Navarro, C. & Doehne, R. (1999). Salt weathering: influence of evaporation rate, supersaturation and crystallization pattern. *Earth Surface Processes and Landforms*. 24, 191-209.

Ruesch, O., Poulet, F., Vincendon, M., Bibring, J., Carter, J., Erkeling, G., Gondet, B., Hiesinger, H., Ody, A., Reiss, D. (2012). Compositional investigation of the proposed chloride-bearing materials on Mars using near-infrared orbital data from OMEGA/Mex. *Journal of Geophysical Research: Planets*. 117.

Ruff, S.W. & Farmer, J.D. (2016). Silica deposits on Mars with features resembling hot spring biosignatures at El Tatio in Chile. *Nature Communications*. 7, doi: 10.1038/ncomms13554.

Ruff, S.W., Farmer, J.D., Calvin, W.M., Herkenhoff, K.E., Johnson, J.R., Morris, R.V., Arvidson, R.E., Bell, J.F., Christensen, P.R., Squyres, S.W. (2011). Characteristics, distribution, origin, and significance of opaline silica observed by the Spirit rover in Gusev crater, Mars. *Journal of Geophysical Research: Planets*. 116, doi: 10.1029/2010JE003767.

Siever, R. (1962). Silica solubility, 0 ° - 200 °C., and the diagenesis of siliceous sediments. *The Journal of Geology*. 70, 127-150.

Squyres, S.W., Arvidson, R.E., Ruff, S., Gellert, R., Morris, R.V., Ming, D.W., Crumpler, L., Farmer, J.D., Des Marais, D.J., Yen, A., McLennan, S.M., Calvin, W., Bell III, J.F., Clark, B.C., Wang, A., McCoy, T.J., Schmidt, M.E., de Souza Jr., P.A. (2008). Detection of silica-rich deposits on Mars. *Science*. 320, 1063-1067, doi: 10.1126/science.1155429.

Squyres, S. W., Grotzinger, J. P., Arvidson, R. E., Bell, J. F., Calvin, W., Christensen, P. R, Clark, B.C., Crisp, J.A., Farrand, W.H., Herkenhoff, K.E., Johnson, J.R., Klingelhofer, G., Knoll, A.H., McLennan, S.M., McSween Jr., H.Y., Morris, R.V., Rice Jr., J.W., Rieder, R., Soderblom, L.A. (2004). In situ evidence for an ancient aqueous environment at Meridiani Planum, Mars. *Science*. 306, 1709-1714.

Squyres, S.W. & Kasting, J.F. (1994). Early Mars: how warm and how wet? *Science*. 265, 744-749, doi: 10.1126/science.265.5173.744.

Stok, J.R., Mustard, J.F., Ehlmann, B.L., Milliken, R.E., Murchie, S.L. (2010). Silica deposits in the Nili Patera caldera on the Syrtis Major volcanic complex on Mars. *Nature Geoscience*. 3, 838-841.

Sutter, B., McAdam, A., Mahaffy, P.R., Ming, D.W., Edgett, K.S., Rampe, E.B., Eigenbrode, J.L., Franz, H.B., Freissinet, C., Grotzinger, J.P., Steele, A., House, C.H., Archer, P.D., Malespin, C.A., Navarro-Gonzalez, R., Stern, J.C., Bell, J.F., Calef, F.J., Gellert, R., Glavin, D.P., Thompson, L.M., Yen, A.S. (2017) Evolved gas analyses of sedimentary rocks and eolian sediment in Gale Crater, Mars: Results of Curiosity rover's sample analysis at Mars instrument from Yellowknife Bay to Namib Dune. *Journal of Geophysical Research: Planets*. 122, 2574-2609, doi: 10.1002/2016JE005225.

Weitz, C.M., Bishop, J.L., Grant, J.A. (2013). Gypsum, opal, and fluvial channels within a trough of Noctis Labyrinthus, Mars: implications for aqueous activity during the late Hesperian to Amazonian. *Planetary and Space Science*. 87, 130-145, doi: 10.1016/j.pss.2013.08.007.

White, D.E., Brannock, W.W., Murata, K.J. (1956). Silica in hot-spring waters. *Geochimica et Cosmochimica Acta*. 10, 27-59.

Data Statement: Data produced in this research is included in tables and figures within this manuscript. SEM images that were not included in this manuscript can be requested from the corresponding author.